

# Application of Relativistic Coupled-cluster Theory to Electron Impact Excitations of $\text{Mg}^+$ in the Plasma Environment

L. Sharma<sup>1</sup>, B. K. Sahoo<sup>2,3</sup>, P. Malkar<sup>1</sup> and R. Srivastava<sup>1</sup>

<sup>1</sup>*Department of Physics, Indian Institute of Technology Roorkee, Roorkee 247667, India*

<sup>2</sup>*Atomic and Molecular Physics Division, Physical Research Laboratory, Navrangpura, Ahmedabad 380009, India*

<sup>3</sup>*State Key Laboratory of Magnetic Resonance and Atomic and Molecular Physics, Wuhan Institute of Physics and Mathematics, Chinese Academy of Sciences, Wuhan 430071, China*

(Dated: October 2, 2018)

A relativistic coupled-cluster (RCC) theory is implemented to study electron impact excitations of atomic species. As a test case, the electron impact excitations of the  $3s\ ^2S_{1/2} - 3p\ ^2P_{1/2,3/2}$  resonance transitions are investigated in the singly charged magnesium ( $\text{Mg}^+$ ) ion using this theory. Accuracies of wave functions of  $\text{Mg}^+$  are justified by evaluating its attachment energies of the relevant states and compared with the experimental values. The continuum wave function of the projectile electron are obtained by solving Dirac equations assuming distortion potential as static potential of the ground state of  $\text{Mg}^+$ . Comparison of the calculated electron impact excitation differential and total cross-sections with the available measurements are found to be in very good agreements at various incident electron energies. Further, calculations are carried out in the plasma environment in the Debye Hückel model framework, which could be useful in the astrophysics. Influence of plasma strength on the cross-sections as well as linear polarization of the photon emission in the  $3p\ ^2P_{3/2} - 3s\ ^2S_{1/2}$  transition is investigated for different incident electron energies.

PACS numbers:

## I. INTRODUCTION

Accurate determination of scattering cross-sections of electrons with atomic systems are of immense interest to a wide range of applications in astrophysics and plasma physics [1–7]. The challenges in the calculations of scattering cross-sections lie in determining accurate wave functions for the ground and excited states of the target as well as calculating wave functions of the scattered electron in the vicinity of the target. Furthermore, it is important to evaluate these wave functions in the relativistic framework to investigate many subtle effects of the problem. Many-body methods in the close-coupling [8] and R-matrix [9] formalisms in the non-relativistic approach, and multi-configuration Dirac-Fock (MCDF) method, which is a special case of a truncated configuration interaction (CI) method, in the relativistic approach are the commonly used [10] techniques to evaluate the wave functions of the target atomic systems. However, a truncated CI method does not include the electron correlation effects in correct scaling with the size of the system [11, 12]. In contrast, a relativistic coupled-cluster (RCC) method is known today as the golden many-body method in the nuclear, atomic and molecular physics for its ability to incorporate the electron correlation effects to all orders in perturbation for evaluating wave functions [11, 12]. A truncated RCC method can still include contributions from higher level excitations even at the same excitation level approximations in the CI method. Moreover, truncated RCC methods obey the size-extensivity and size-consistent behaviors. It, thus, would be interesting to apply the RCC method to electron-atom scattering problems and compare the results with the available experimental and other theoretical calculations.

On the other hand, study of atomic processes in plasma environment has received great attention in recent years due to its importance in understanding different physical processes involved in varieties of low to high temperature plasma (see a review [13] and references therein). Most of such plasmas contain different charged species as well as free electrons which screen the atomic potential of the embedded atomic systems (neutral atoms or ions) as well as influence the collisional processes therein [14–16]. As a result, there are deviations in the structures of the atomic systems and associated collisional parameters from their corresponding behavior in the absence of plasma environment [16–18]. It is, therefore, important to understand the influence of the plasma environment on the atomic systems for plasma diagnostic purposes. However, studying the electronic structures of atomic systems immersed in plasma environment is quite challenging and the accurate evaluation of the electronic structures of atoms or ions as well as adequate description of the atomic processes involved can be said to be one of the most demanding research in the recent years due to their wide range of applications. To determine atomic wave functions of the plasma embedded atomic systems, a suitable model is required which can account for the appropriate screening effects of the Coulomb potentials. Moreover, it is necessary to employ a many-body method that can include both the electron-electron correlations and relativistic effects rigorously. For this purpose various models have been proposed and used; viz., ion sphere model, Thomas Fermi model, Debye-Hückel model, etc. [16, 19–21]. For low density and high temperature plasma, the Debye-Hückel model is found to be quite reliable to describe the influence of the screened Coulomb potentials in the calculations of atomic structure and collision pa-

rameters [16].

In any plasma the most dominant collision process that can occur is due to electron impact on atomic species causing excitation and ionization processes. So far, there have been some efforts to understand the effects of plasma environment on the elastic and inelastic scattering of electrons from H-like and He-like ions [22–28]. However, most of such studies have been restricted to the total excitation cross-sections. It is only recently that Chen et al [29] applied a fully relativistic distorted wave theory to study the influence of Debye plasma on the magnetic cross-section and linear polarization of X-ray radiation following inner-shell electron-impact excitation of highly charged Be-like ions. Therefore, there is in general lack of studies related to the plasma screening effects on electron impact excitation of many-electron atomic systems and even so, for their magnetic sublevel cross-sections, and characteristic photon emission during the radiative de-excitation processes.

There are two fold objectives here; first, to achieve accurate description of the electronic structure of many-electron atomic species and then, extending it to study the electron impact excitations of these atoms in the Debye plasma description so that collisional process can also be described to the same degree of accuracy. The RCC method has been widely applied for high precision atomic structure calculations [30–33]. In this work, we intend to employ this method to calculate the amplitudes of the electron excitations of atomic systems. For illustration, we consider a singly charged magnesium ion ( $\text{Mg}^+$ ) to study electron impact excitation of its  $3s^2S_{1/2} - 3p^2P_{1/2,3/2}$  resonant transitions in the plasma environment with the Debye-Hückel model framework. These resonance lines yield important emission features in the spectra of active galactic nuclei and provide information about intervening materials along the line of sight [34–36]. Since magnesium is one of the most abundant elements in the Galaxy, variation in the intensity of the spectral lines of the above transitions can act as diagnostic tools to determine the physical conditions of interstellar clouds. Thus, for further understanding of the interstellar medium, it is important to study the electron impact excitations of the first excited state fine-structure splitting from the ground ( $3s^2S_{1/2}$ ) state of the  $\text{Mg}^+$  ion in the plasma environment. These transitions exist naturally in many astrophysical objects [37, 38]. So far, a few theoretical and experimental investigations have been de-

voted to understand excitation processes in the plasma isolated  $\text{Mg}^+$  ion [39–44]. However, such studies have never been carried out for plasma embedded  $\text{Mg}^+$ . From this point of view, we perform calculations of differential cross-sections (DCS), integrated cross-sections (ICS) and polarization of characteristic photon emission as function of Debye length considering various incident electron energies ranging from 10 to 100 eV. To obtain these results accurately, it is imperative to evaluate both the bound and continuum wave functions by including the Debye-Hückel interaction potentials accounting for the plasma screening effects at various plasma strengths.

In the point of view of above, we have implemented and used the RCC method in the singles and doubles excitation approximation (CCSD method) to obtain the scattering amplitudes of the electron from the  $\text{Mg}^+$  ion at various plasma strengths. The wave functions of the initial and final states of the  $\text{Mg}^+$  ion are evaluated in the similar approach adopted to study ionization potential depressions (IPD) of the plasma embedded atomic systems [45, 46]. Also, our previously reported RDW method [39] is extended further to calculate the wave function of the scattered electron in the vicinity of the plasma embedded atomic systems. We consider the Debye-Hückel screening potential model and solve the coupled Dirac equations using distortion potential, which is taken as the spherically averaged static potential of the target ion.

This paper is organized as follows: Method of calculations for the scattered electron and target wave functions in the plasma environment as well as evaluation of scattering amplitude are mentioned briefly in Sec. II. In Sec. III, we present results and their discussions following the concluding remarks in Sec. IV. Unless stated otherwise, we adopt the atomic units (a.u.) throughout the paper.

## II. THEORY AND METHODOLOGY

### A. Theory of scattering amplitude

Within the relativistic distorted wave approximation the first order direct scattering amplitude for electron impact excitation of an ion having nuclear charge  $Z$  and number of electrons  $N$  from its initial state  $|\Psi_i\rangle$  to final state  $|\Psi_f\rangle$  can be expressed as

$$f(J_i, M_i, \mu_i; J_f, M_f, \mu_f, \theta) = 4\pi^2 \sqrt{\frac{k_f}{k_i}} \langle \Psi_f(\mathbf{1}, \mathbf{2}, \dots, \mathbf{N}) F_f^{DW-}(\mathbf{k}_f, \mathbf{N}+1) | V_{in} - V_d(r_{N+1}) | \Psi_i(\mathbf{1}, \mathbf{2}, \dots, \mathbf{N}) F_i^{DW+}(\mathbf{k}_i, \mathbf{N}+1) \rangle. \quad (1)$$

In this amplitude the ionic states are uniquely spec-

ified with well-defined total angular momentum  $J$  and

its magnetic component  $M$ , whereas spin projections of the projectile and scattered electrons are denoted respectively, by  $\mu_i$  and  $\mu_f$ .  $|\Psi_{i,f}(N)\rangle$  show the  $N$ -electron target wave functions having position coordinates with respect to the nucleus as  $r_j$ , where  $j = 1, 2, \dots, N$ , and  $F_{i,f}^{DW+(-)}$  with position coordinate  $r_{N+1}$  represent the incident or scattered electron and its superscript  $DW$  means they are determined by the distorted wave function approximation. In our RDW method, they are calculated in the presence of a suitably defined distortion potential  $V_d$ . Here  $- (+)$  signs refer to the incoming

(outgoing) waves with their relativistic wave numbers  $k_i$  ( $k_f$ ). In Eq. (1),  $V_{in}$  is the screened Coulomb interaction between the projectile electron and the target ion. The geometry of the scattering process is chosen so that the direction of the incident electron defines the  $z$  axis and  $xz$  plane forms the scattering plane. Therefore, the scattering angle  $\theta$  is the angle between the wave vectors  $\mathbf{k}_i$  and  $\mathbf{k}_f$  of the incident and scattered electrons.

In order to evaluate the scattering amplitude, Eq. (1) can be casted into the following form

$$f(J_i, M_i, \mu_i; J_f, M_f, \mu_f, \theta) = 4\pi^2 \sqrt{\frac{k_f}{k_i}} \left\langle F_f^{DW-}(\mathbf{k}_f, \mathbf{N}+1) | U_{i \rightarrow f}(r_{N+1}) | F_i^{DW+}(\mathbf{k}_i, \mathbf{N}+1) \right\rangle, \quad (2)$$

where

$$U_{i \rightarrow f}(r_{N+1}) = \left\langle \Psi_f(\mathbf{1}, \mathbf{2}, \dots, \mathbf{N}) | V_{in} | \Psi_i(\mathbf{1}, \mathbf{2}, \dots, \mathbf{N}) \right\rangle. \quad (3)$$

In the following subsections we describe in detail various constituents that are required to evaluate the above scattering amplitude.

## B. Coulomb potentials

The atomic electrons as well as free electrons will experience the screening of electron-nucleus as well as electron-electron Coulomb interactions. Therefore,  $V_{in}$  can be written as

$$V_{in}(r_i, r_j) = V_n(r_i) + V_{ee}(r_{ij}), \quad (4)$$

where  $V_n(r_i)$  and  $V_{ee}(r_{ij})$  represent, respectively, the interaction of bound or free  $i^{th}$  electrons with atomic nucleus and the other  $j^{th}$  electron. In the following we discuss the general forms, as described by Debye-Hückle model, for  $V_n(r_i)$  and  $V_{ee}(r_{ij})$  that are used in the present work to evaluate the scattering amplitude as well as in obtaining the target and projectile electron wave functions in the plasma. The same can also be deduced for the plasma free systems by taking special conditions.

In the weakly coupled plasma, an electron of the plasma embedded atomic system located at  $r_i$  can see the screened nuclear potential with Fermi nuclear charge distribution as

$$V_n(r_i) = -\frac{Ze^{-r_i/D_l}}{\mathcal{N}r_i} \times \begin{cases} \frac{1}{b} \left( \frac{3}{2} + \frac{a^2\pi^2}{2b^2} - \frac{r^2}{2b^2} + \frac{3a^2}{b^2} P_2^+ + \frac{6a^3}{b^2\pi^2} (S_3 - P_3^+) \right) & \text{for } r_i \leq b \\ \frac{1}{r_i} \left( 1 + \frac{a^2\pi^2}{b^2} - \frac{3a^2r}{b^3} P_2^- + \frac{6a^3}{b^3\pi^2} (S_3 - P_3^-) \right) & \text{for } r_i > b. \end{cases} \quad (5)$$

Here  $D_l$  refers to the Debye length expressed as

$$D_l = \sqrt{\frac{k_B T_e}{4\pi(1+z_i)n_e}}, \quad (6)$$

where  $k_B$  is the Boltzmann constant,  $n_e$  is the electron density,  $T_e$  is the temperature and  $z_i$  is charge of the target in the plasma. In Eq. (5) the various factors are given by

$$\begin{aligned} \mathcal{N} &= 1 + \frac{a^2\pi^2}{b^2} + \frac{6a^3}{b^3} S_3 \\ \text{with } S_k &= \sum_{l=1}^{\infty} \frac{(-1)^{l-1}}{l^k} e^{-lb/a} \\ \text{and } P_k^{\pm} &= \sum_{l=1}^{\infty} \frac{(-1)^{l-1}}{l^k} e^{\pm l(r-b)/a}. \end{aligned} \quad (7)$$

In the above expressions,  $b$  is known as the half-charge radius and  $a = 2.3/4(\ln 3)$  is related to the skin thickness of the nucleus. The parameter  $b$  is evaluated using the relation

$$b = \sqrt{\frac{5}{3} r_{rms}^2 - \frac{7}{3} a^2 \pi^2}, \quad (8)$$

with the appropriate value of the root mean square radius of the nucleus  $r_{rms}$ , which is estimated using the empirical formula

$$r_{rms} = 0.836A^{1/3} + 0.570, \quad (9)$$

in fm for the atomic mass  $A$ .

The screened two-body Coulomb potential within the

atomic system can be expressed as

$$\begin{aligned} V_{ee}(r_{ij}) &= \sum_{j \geq i}^N \frac{e^{-|r_i - r_j|/D_l}}{|r_i - r_j|} \\ &= \frac{4\pi}{\sqrt{r_i r_j}} \sum_{k=0}^{\infty} I_{k+\frac{1}{2}}(r_{<}/D_l) K_{k+\frac{1}{2}}(r_{>}/D_l) \\ &\quad \times \sum_{q=-k}^k Y_q^{k*}(\theta, \phi) Y_q^k(\theta, \phi), \end{aligned} \quad (10)$$

where  $I_{k+\frac{1}{2}}(r)$  and  $K_{k+\frac{1}{2}}(r)$  are the modified Bessel functions of the first and second kind, respectively, with  $r_{>} = \max(r_i, r_j)$ ;  $r_{<} = \min(r_i, r_j)$ , and  $Y_q^k(\theta, \phi)$  is the spherical harmonics of rank  $k$  with its component  $q$ . In terms of the Racah operator ( $C_q^k$ ), the above expression is given by a scalar product as

$$\begin{aligned} V_{ee}(r_{ij}) &= \frac{1}{\sqrt{r_i r_j}} \sum_{k=0}^{\infty} (2k+1) I_{k+\frac{1}{2}}(r_{<}/D_l) K_{k+\frac{1}{2}}(r_{>}/D_l) \\ &\quad \times \mathbf{C}^k(\hat{r}_i) \cdot \mathbf{C}^k(\hat{r}_j). \end{aligned} \quad (11)$$

Similarly, the screened two-body Coulomb potential for interaction of projectile electron with atomic electrons can be expressed as

$$V_{ee}(r_{j,N+1}) = \sum_{j=1}^N \frac{e^{-|r_j - r_{N+1}|/D_l}}{|r_j - r_{N+1}|}. \quad (12)$$

This expression can further be written as multipole expansion in the same way as done above in Eq. (10).

It to be noted that in the plasma free system,  $n_e = 0$ , so  $D_l \rightarrow \infty$ . Considering this special condition, results for the plasma isolated systems are obtained.

### C. RCC method for the wave functions of the target

In the relativistic framework, the wave functions of the target is determined by considering the Dirac-Coulomb (DC) Hamiltonian, which is given by

$$H = \sum_{i=1}^N \left[ c\boldsymbol{\alpha}_i \cdot \mathbf{p}_i + (\beta_i - 1)c^2 + V_n(r_i) + \sum_{j \geq i} V_{ee}(r_{ij}) \right],$$

where  $\boldsymbol{\alpha}$  and  $\beta$  are the Dirac matrices and  $c$  is the velocity of light.

The initial and final states of the considered target  $\text{Mg}^+$  has been calculated by expressing them as a common inert core, i.e.  $[2p^6]$ , and a valence electron in the respective states. Conveniently, we obtain first the single particle orbitals of the closed-core employing the Dirac-Hartree-Fock (DHF) method. The wave functions of the exact states are evaluated by using the exponential *ansatz* in the RCC theory as

$$|\Psi_v\rangle = e^T \{1 + S_v\} |\Phi_v\rangle, \quad (13)$$

where  $|\Phi_v\rangle = a_v^\dagger |\Phi_0\rangle$ , for the DHF wave function of the closed-core  $|\Phi_0\rangle$ . Here,  $T$  and  $S_v$  are the RCC excitation operators that excite electrons from  $|\Phi_0\rangle$  and  $|\Phi_v\rangle$ , respectively, to the virtual space. It can be noted that the above expression is linear in  $S_v$  operator owing to presence of only one valence orbital  $v$  in  $|\Phi_v\rangle$ . This expression is, however, exact and it accounts for the non-linear effects through the products of  $T$  and  $S_v$  operators. In the CCSD method approximation, the RCC operators are expressed as  $T = T_1 + T_2$  and  $S_v = S_{1v} + S_{2v}$  with the subscripts 1 and 2 referring to the singly and doubly excited state configurations, respectively. The amplitudes of these RCC operators are evaluated by solving the following coupled-equations

$$\langle \Phi_0^* | \bar{H} | \Phi_0 \rangle = 0 \quad (14)$$

and

$$\langle \Phi_v^* | (\bar{H} - \Delta E_v) S_v | \Phi_v \rangle = -\langle \Phi_v^* | \bar{H}_N | \Phi_v \rangle, \quad (15)$$

where  $|\Phi_0^*\rangle$  and  $|\Phi_v^*\rangle$  are the excited state configurations, here up to doubles, with respect to the DHF wave functions  $|\Phi_0\rangle$  and  $|\Phi_v\rangle$  respectively. Here  $\bar{H} = (He^T)_c$  with subscript  $c$  represents for the connected terms only and  $\Delta E_v$  is the electron attachment energy (EA), which is equivalent to second ionization potential (IP), of the electron of the valence orbital  $v$ . We evaluate  $\Delta E_v$  by

$$\Delta E_v = \langle \Phi_v | \bar{H} \{1 + S_v\} | \Phi_v \rangle - \langle \Phi_0 | \bar{H} | \Phi_0 \rangle. \quad (16)$$

Both Eqs. (15) and (16) are solved simultaneously, as a result Eq. (15) effectively becomes non-linear in the  $S_v$  operator. In fact, the excitation energy (EE) between two given states is evaluated by taking difference between the respective EAs obtained from the above procedure.

After obtaining amplitudes of the RCC operators using the above described equations, the matrix element of  $V_{in}$  between the states  $|\Psi_i\rangle$  and  $|\Psi_f\rangle$ , i.e. Eq. (3), is evaluated using the expression

$$\begin{aligned} U_{i \rightarrow f}(r_{N+1}) &= \langle \Psi_f | V_{in} | \Psi_i \rangle \\ &= \frac{\langle \Phi_f | \tilde{V}_{in} | \Phi_i \rangle}{\sqrt{\langle \Phi_f | \{1 + \tilde{N}_f\} | \Phi_f \rangle \langle \Phi_i | \{1 + \tilde{N}_i\} | \Phi_i \rangle}}, \end{aligned} \quad (17)$$

where  $\tilde{V}_{in} = \{1 + S_f^\dagger\} e^{T^\dagger} V_{in} e^T \{1 + S_i\}$  and  $\tilde{N}_{k=f,i} = \{1 + S_k^\dagger\} e^{T^\dagger} e^T \{1 + S_k\}$ . As can be seen, it involves two non-terminating series in the numerator and denominator in the above expression, which are  $e^{T^\dagger} V_{in} e^T$  and  $e^{T^\dagger} e^T$  respectively. We adopt iterative procedures to account for contributions from these non-terminating series as have been described in our earlier works on the plasma isolated systems [32, 33].

TABLE I: EAs (in eV) and EEs (in eV) as function of  $D_l$  (in a.u.) in the plasma embedded  $\text{Mg}^+$  ion. Results for the plasma free ( $D_l \rightarrow \infty$ ) are compared with the NIST data [47].

$D_l$	EE				EA	
	$3s^2S_{1/2} - 3p^2P_{1/2}$	$3s^2S_{1/2} - 3p^2P_{3/2}$	$3s^2S_{1/2} - 3p^2P_{3/2}$	$3s^2S_{1/2} - 3p^2P_{3/2}$	$3s^2S_{1/2} - 3p^2P_{3/2}$	$3s^2S_{1/2} - 3p^2P_{3/2}$
$\infty$	4.4162	4.4224	4.4283	4.4348	7.6909	7.6460
100	4.4142	-	4.4263	-	7.4208	-
10	4.2489	-	4.2599	-	5.1766	-
7.0	4.0908	-	4.1007	-	4.2408	-
5.75	3.9472	-	3.9562	-	3.6205	-
3.80	3.3953	-	3.4012	-	2.1173	-
2.865	2.6089	-	2.6111	-	1.0679	-
2.863	2.6061	-	-	-	1.0655	-

#### D. RDW method for the wave functions of the scattered electron

The distortion potential  $V_d$  is taken to be the spherically averaged static potential of the ion in its initial state. It can be expressed as

$$V_d = \left\langle \Psi_i(\mathbf{1}, \mathbf{2}, \dots, \mathbf{N}) \left| V_n(r_{N+1}) + \sum_{j=1}^N V_{ee}(r_{j, N+1}) \right| \Psi_i(\mathbf{1}, \mathbf{2}, \dots, \mathbf{N}) \right\rangle. \quad (18)$$

After substituting  $V_{ee}$  from Eq. (10) with  $k = 0$ ,  $V_d$  is given by

$$V_d(r_{N+1}) = V_n(r_{N+1}) + \pi \sum_{j=1}^N \int \frac{1}{\sqrt{r_j r_{N+1}}} \sqrt{\frac{r_{<}}{r_{>}}} \times \sinh(r_{<}/D_l) e^{-r_{>}/D_l} |\Psi_i|^2 dr_j dr_{N+1}. \quad (19)$$

It is assumed that the atomic wave functions are not distorted by the projectile electron. The relativistic partial wave expansion, as described in our previous work [39], has been used for distorted wave functions  $F_{i,f}^{DW+(-)}$  of the projectile electron. For each partial wave, the large and small components of the continuum wave functions are obtained by solving the coupled Dirac equations using  $V_d$  potential [39]. Thus, scattering amplitude given by Eq. (2) can finally be evaluated using both the partial wave expansion and the matrix element given by Eq. (17).

#### E. Scattering Parameters

After obtaining the scattering amplitude, the relevant parameters related to the electron-atom collision process can be calculated. With our normalization of the distorted waves, the DCS for excitation of ion from initial

state  $i$  to final state  $f$  is given by

$$\frac{d\sigma(\theta)}{d\Omega} = \frac{1}{2(2J_i + 1)} \sum_{\substack{M_i, \mu_i \\ M_f, \mu_f}} |f(J_i, M_i, \mu_i; J_f, M_f, \mu_f, \theta)|^2. \quad (20)$$

In the above expression, we have summed over the spins of the incident and scattered electron as well as magnetic quantum numbers corresponding to the total angular momenta of the ion in the initial and final states. The ICS (denoted by  $\sigma$ ) is obtained by integrating the DCS over all the scattering angles. However, if averaging is done over initial magnetic sublevels  $M_i$ , cross-section for excitation to a specific final magnetic sublevel  $M_f$  can be calculated (denoted by  $\sigma_{M_f}$ ). Using the magnetic sublevel cross-sections, the degree of linear polarization of the photon emission can be obtained. Here we consider excitations from the  $3s^2S_{1/2}$  ground state to the  $3p^2P_{1/2}$  and  $3p^2P_{3/2}$  levels and subsequent decay from the  $3p^2P_{3/2}$  level to the ground state by emitting a photon. Since in the electron-photon coincidence experiments the photon is detected in the direction perpendicular to the scattering plane, the linear polarization of the emitted photon can be obtained using the  $\sigma_{M_f}$  values of the excited state, i.e.,

$$P = \frac{3(\sigma_{1/2} - \sigma_{3/2})}{3\sigma_{3/2} + 5\sigma_{1/2}}. \quad (21)$$

The linear polarization of the photon emitted due to decay from the  $3p^2P_{1/2}$  level to the  $3s^2S_{1/2}$  state will be zero, since cross-sections for the magnetic sublevels  $M_f = \pm 1/2$  are equal.

### III. RESULTS AND DISCUSSION

We present here our relativistic calculations for electron impact excitations of the  $3s^2S_{1/2}$  to  $3p^2P_{1/2}$  and  $3p^2P_{3/2}$  states in  $\text{Mg}^+$ . We have obtained the DCS, ICS and linear polarization results for isolated as well as plasma embedded  $\text{Mg}^+$ . It is evident that the reliability of the collision parameters depends crucially on the accuracies of the wave functions used in the calculations. Therefore, in Table I we have compared the RCC results for EAs and EEs for the considered states in the present work with the corresponding experimental values quoted in the NIST database [47]. We find that our results are in excellent agreement with the NIST data. We have also calculated these quantities at various  $D_l$  values for which no other theoretical or experimental results are available to compare. These  $D_l$  values can correspond to different plasma conditions with varying temperature or varying electron density that are of general interest. We notice that our EAs and EEs decrease with decreasing value of  $D_l$ . This feature is in confirmation with earlier studies revealing IPD of the atomic systems in plasma environment [45]. It can be further be seen from the Table I

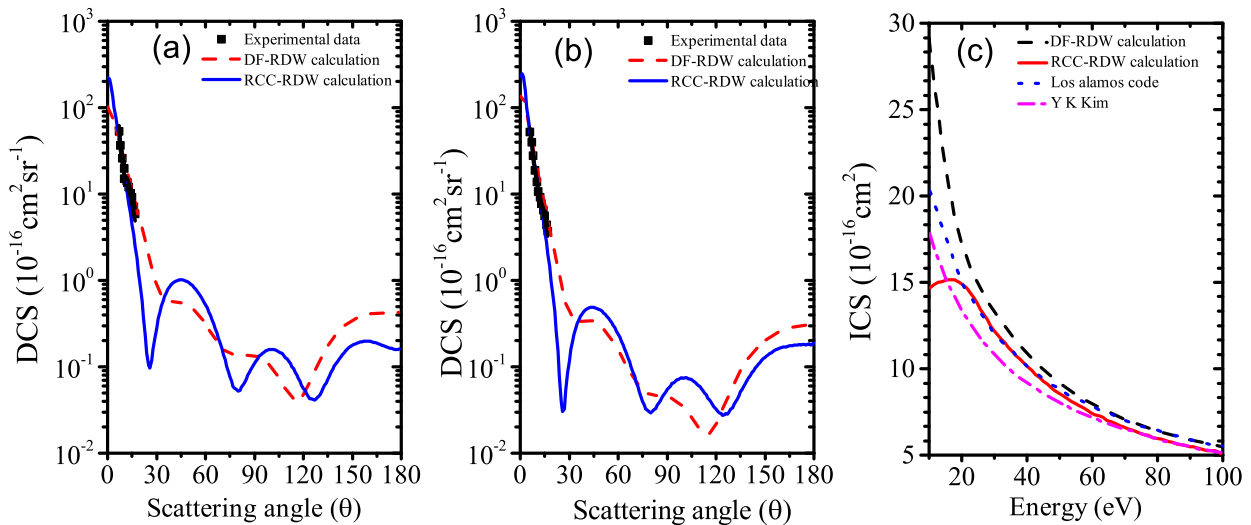


FIG. 1: (Color online) Electron impact excitations of the  $3s \ ^2S_{1/2} \rightarrow 3p \ ^2P_{1/2}$  and  $3s \ ^2S_{1/2} \rightarrow 3p \ ^2P_{3/2}$  transitions of  $\text{Mg}^+$  ion. We show (a) DCS at 35 eV (b) DCS at 50 eV and (c) ICS with solid curve representing the RCC-RDW calculations, dashed curves for the DF-RDW calculations [39], short dashed curves for the calculations with the Los Alamos code [49], and dashed-dotted curves for the scaled results from Ref. [43]. The available experimental values are shown by points with error bars that were reported in Refs. [41, 42].

that there is no result presented at  $D_l = 2.863$  a.u. for excitation energy of the  $3p \ ^2P_{3/2}$  state. This is due to the reason that a slight change in the value of  $D_l$  from 2.865 to 2.863 leads to the conversion of the bound  $3p \ ^2P_{3/2}$  state into a continuum state.

As mentioned already in Introduction, the RCC method is employed for the first time to study the collisional excitation of atoms and hence, for understanding the influence of plasma environment on collisional parameters. Therefore, it is worth to compare the new cross-section results, which we denote as RCC-RDW, using RCC wave functions with the previously available theoretical and experimental results. To this effect, in Figs. 1(a) and (b) our DCS results are shown, respectively, at 35 eV and 50 eV and are compared with the experimental data of Williams et al [41, 42] and previous RDW calculations [39]. Since the measurements [41, 42] have been reported for the sum of the cross-sections for the transition from  $3s \ ^2S_{1/2}$  to  $3p \ ^2P_{3/2}$  and  $3p \ ^2P_{1/2}$  states, we have presented the summed DCSs in Figs. 1(a) and (b). For the sake of clarity we have not included old theoretical results from non-relativistic distorted wave [44] and 5 state close-coupling [42] methods. We have already reported detailed comparison of RDW results with these non-relativistic calculations and measurements in our previous work for singly charged metal ions including  $\text{Mg}^+$  [39]. The difference between present RCC-RDW and old RDW calculations [39] is due to the inclusion of higher correlation effects in our RCC method that is used in the present calculations to obtain bound state wave functions of the  $\text{Mg}^+$  ion. Earlier, these wave functions were obtained using the MCDF method from the readily available GRASP92 code [48]. Therefore, we refer to these results here as DF-RDW calculations. It can be seen from Figs. 1(a) and (b) that our RCC-RDW results are in good agreement with the DF-RDW calculations and the measurements, which are available up

to  $20^0$  scattering angles. The disagreement between the shape of the theoretical DCS curves is more after  $20^0$  scattering angles. It could be due to accounting electron correlation effects in the RCC method, especially the core-polarization effects, to all orders in perturbation. The shortcoming of the MCDF method is that it cannot incorporate core-polarization effects rigorously. Therefore, we believe that the present RCC-RDW results are improved ones that need to be investigated by the future experiments. This demands for more measurements at large scattering angles to confirm the shapes of the DCS curves. In Fig. 1(c), we have compared our summed ICS results with the DF-RDW calculations, scaled cross-sections of Kim [43] as well as semi-relativistic distorted wave calculations from the Los Alamos code [49]. The agreement of the new ICS curve is better with Kim's results in the entire energy range and it improves with increasing incident energy of the electron.

In Fig. 2, we have shown the DCS results at incident electron energy ranging from 20 to 100 eV and various Debye lengths viz.,  $D_l = 100, 10, 7, 5.75, 3.8, 2.865$  and  $2.863$  a.u.. The left and right panels exhibit DCS results, respectively, for the  $3^2S_{1/2}$  to  $3^2P_{1/2}$  and  $3^2S_{1/2}$  to  $3^2P_{3/2}$  transitions. Since  $3^2P_{3/2}$  state does not remain a bound state for  $D_l < 2.865$  a.u., there is no DCS displayed for excitation of this state at  $D_l < 2.863$  a.u.. Further, we find that at  $D_l = 100$  a.u., the DCS curves overlap with those at  $D_l = \infty$ , which corresponds to no plasma screening, at all the projectile electron energies. As the value of  $D_l$  decreases, the DCS decreases consistently while maintaining the similar shape of the curves approximately beyond  $10^0$  scattering angles. This can be attributed to the fact that the screening of nuclear charge increases with decreasing Debye length, causing a drop in the value of the cross-sections. The maxima of the DCS curves fall by two orders of magnitude in the considered range of Debye length. Moreover, in the forward

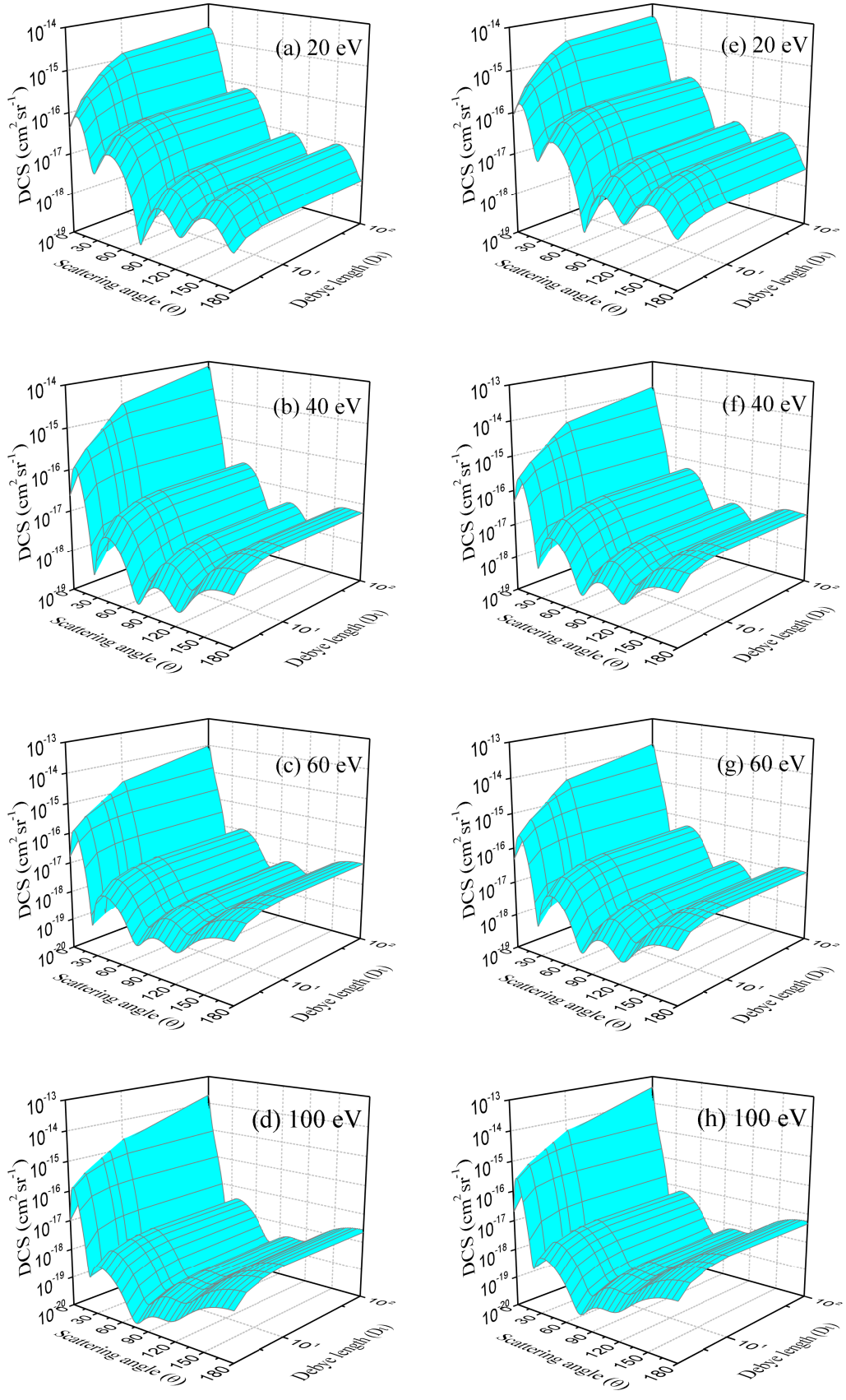


FIG. 2: (Color online) Demonstration of variations in DCSs at various Debye lengths as function of incident electron energy for the excitations from the  $3^2S_{1/2}$  state to the  $3^2P_{1/2}$  and  $3^2P_{3/2}$  states that are shown in the left and right panels, respectively.

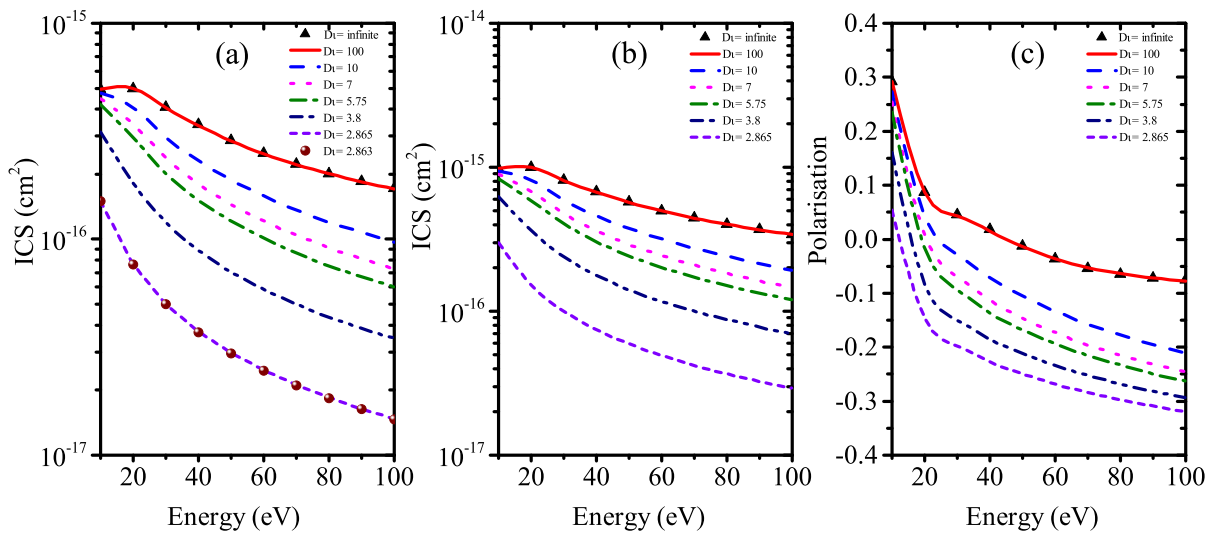


FIG. 3: (Color online) Demonstration of ICSs for the electron impact excitations in the plasma embedded  $\text{Mg}^+$  ion. Results shown in (a) for the  $3s \ ^2S_{1/2} \rightarrow 3p \ ^2P_{1/2}$  transition and shown in (b) for the  $3s \ ^2S_{1/2} \rightarrow 3p \ ^2P_{3/2}$  transition. Results shown in (c) are the polarization fractions for the  $3p \ ^2P_{3/2}$  to  $3s \ ^2S_{1/2}$  transition.

scattering angle region up to  $10^\circ$ , the shapes of the DCS curves for  $D_l \leq 10$  a.u. is significantly different from that at  $D_l = 100$  a.u.. Particularly, at incident electron energies greater than 40 eV, the DCS at  $D_l = 100$  a.u. shows a sharp forward peak which is characteristic of allowed transition, whereas, DCS at  $D_l \leq 10$  a.u. exhibit a broad peak at around  $5^\circ$ , a well known feature of dipole forbidden transitions.

The ICS for excitation of the ground state  $3^2S_{1/2}$  to the excited states  $3^2P_{1/2}$  and  $3^2P_{3/2}$  are displayed, respectively, in Figs. 3(a) and (b). These results are shown for isolated ion as well as for various Debye lengths  $D_l$  ranging from 2.863 to 100 a.u. for  $^2P_{1/2}$  state and from 2.865 to 100 a.u. for the  $3p \ ^2P_{3/2}$  state. The ICSs at  $D_l = 100$  a.u. are close to those for plasma-free ion. As observed for the DCS curves, the values of ICS also decrease with increasing plasma strength i.e., decrease in the value of  $D_l$ . The effect of plasma screening on the degree of linear polarization  $P$  of the characteristic photon emitted due to decay of the  $3p \ ^2P_{3/2}$  state to the ground  $3s \ ^2S_{1/2}$  state is presented in Fig. 3(c). It can be observed that at 10 eV as  $D_l$  decreases from 100 to 2.865 a.u., the value of  $P$  decreases from 29% to 5%. In the isolated  $\text{Mg}^+$ , the polarization curve crosses zero at about 45 eV. However, in case of plasma embedded  $\text{Mg}^+$  it passes through zero at smaller values of energies with increasing plasma strength. This indicates that the magnetic sub-state with  $M_f = 3/2$  gets more populated as compared to that with  $M_f = 1/2$  in the plasma environment. Moreover, the absolute value of  $P$  increases significantly showing enhancement of polarization to a value close to 32% at 100 eV.

#### IV. CONCLUSION

We have applied the combined RCC theory and RDW method to study the electron impact excitations of the resonant transitions, i.e.  $3s \ ^2S_{1/2}$  to  $3p \ ^2P_{1/2}$  and

$3p \ ^2P_{3/2}$  transitions, in the  $\text{Mg}^+$  ion. Excellent agreement of the attachment and excitation energies with the corresponding experimental values confirm on the accuracies of the wave functions of the ion obtained using the RCC theory. Observation in the depression of the ionization potential in the  $\text{Mg}^+$  ion indicates about the effects of the plasma environment on the atomic structure. Very good agreements between the present DCS results at 35 and 50 eV with the available measurements and DF-RDW calculations in the plasma isolated  $\text{Mg}^+$  ion indicate on the reliability of our calculations. Observed differences between the RCC-RDW and DF-RDW results at large scattering angles demand to ascertain them by carrying out further measurements. This can test validity of the many-body methods. Nevertheless, reasonable agreements between our theoretical results with the available experimental data suggest that results obtained in the plasma embedded ion are of similar accuracies. Results for the plasma embedded ion are reported as function of Debye length  $D_l$  for the DCS, ICS and linear polarization of the photon emission after decay of the  $3p \ ^2P_{3/2}$  state to the ground state at the incident electron energy ranging from 10 to 100 eV. It is observed from our analysis that presence of plasma environment affect the shape of the DCS curves in the small scattering angle range such that the maxima of the DCS curves shifts from  $0^\circ$  towards  $10^\circ$  with decreasing Debye length. It is also found that the cross-sections decrease with decreasing value of  $D_l$ . There is enhancement in the degree of linear polarization of the photon emission as the incident electron energy and plasma screening strength increase. These data could be useful for the plasma diagnostic processes in the astrophysical and laboratory plasmas.

#### Acknowledgements

B. K. S. thanks Dr. Madhulita Das for many useful discussions and acknowledges financial support from CAS



through the PIFI fellowship under the project number 2017VMB0023. L. S. and R. S. acknowledge the support from the Department of Science and Technology (DST),

New Delhi for this work. P. M. is thankful to Ministry of Human Resource and Development (MHRD) for providing her research assistantship.

- 
- [1] A. K. Pradhan and S. N. Nahar, *Atomic Astrophysics and Spectroscopy*, Cambridge University Press, New York (2011).
- [2] R. E. Johnson, *Introduction to Atomic and Molecular Collisions*, Plenum Press, New York and London, (1982).
- [3] M. Y. Amusia, *Many-body effects in single photoionization processes*, Many-body atomic physics, Chapter 8, pg. 185, edited by J. J. Boyle and M. S. Pindzola, Cambridge University Press, New York (1998).
- [4] D. E. Post, *J. Nucl. Mat.* **220**, 143 (1995).
- [5] R. A. Dressler, Yu-hui Chiu, O. Zatsarinny, K. Bartschat, R. Srivastava, and L. Sharma, *J. Phys. D* **42**, 185203 (2009).
- [6] Dipti, R. K. Gangwar, R. Srivastava and A. D. Stauffer, *Eur. J. Phys. D* **67**, 40244 (2013).
- [7] N. R. Badnell, G. Del Zanna, L. Fernandez-Mencherero, A. S. Giunta, G. Y. Liang, H. E. Mason, and P. J. Storey, *J. Phys. B* **49**, 094001 (2016).
- [8] I. Bray, D. V. Fursa, A. S. Kheifets and A. T. Stelbovics, *J. Phys. B* **35**, 15 (2002).
- [9] P. G. Burke, *R-Matrix Theory of Atomic Collisions*, Springer-Verlag Publication, Berlin (2013).
- [10] P. Jönsson, X. He, C. F. Fischer, and I. P. Grant, *Comput. Phys. Commun.* **177**, 597 (2007).
- [11] A. Szabo and N. Ostlund, *Modern Quantum Chemistry*, Dover Publications, Inc., Mineola, New York, First edition (revised), 1996.
- [12] I. Shavitt and R. J. Bartlett, *Many-body methods in Chemistry and Physics*, Cambridge University Press, Cambridge, UK (2009).
- [13] R. K. Janev, S. Zhang, and J. Wang, *Matter Radiat. Extremes* **1**, 237 (2016).
- [14] D. Salzmann, *Atomic Physics in Hot Plasmas*, Oxford University Press, Oxford (1998).
- [15] J. C. Weisheit, *Adv. At. Mol. Phys.* **25**, 101 (1989).
- [16] M. S. Murillo, and J. C. Weisheit, *Phys. Rep.* **302** 1 (1998).
- [17] B. Saha and S. Fritzsche, *Phys. Rev. A*, **73**, 036405 (2006).
- [18] A. N. Sil, J. Anton, S. Fritzsche, P. K. Mukherjee, and B. Fricke, *Eur. Phys. J. D* **55**, 645 (2009).
- [19] Y. Jianmin, *Phys. Rev. E* **66**, 047401 (2002).
- [20] S. Ichimaru, *Rev. Mod. Phys.* **54**, 1017 (1982).
- [21] A. N. Sil, S. Canuto and P. K. Mukherjee, *Spectroscopy of Confined Atomic Systems: Effect of Plasma*, Advances in Quantum Chemistry, Chapter 4, pg. 115, Vol. 58 (2009).
- [22] M. C. Zammit, D. V. Fursa, and I. Bray, *Chem. Phys.* **398**, 214 (2012).
- [23] M. C. Zammit, D. V. Fursa, and I. Bray, *Chem. Phys.* **82**, 052705 (2010).
- [24] S. B. Zhang, J. G. Wang and R. K. Janev, *Phys. Rev. Lett.* **104**, 023203 (2010).
- [25] S. B. Zhang, J. G. Wang, R. K. Janev and X. J. Chen, *Phys. Rev. A* **83**, 032724 (2011).
- [26] Y. Y. Qi, Y. Wu, J. G. Wang and Y. Z. Qu, *Phys. Plasmas* **16**, 023502 (2009).
- [27] Y. Y. Qi, J. G. Wang and R. K. Janev, *Phys. Rev. A* **80**, 063404 (2009).
- [28] A. Ghoshal and Y. K. Ho, *J. Phys. B* **43**, 045203 (2010).
- [29] Z. B. Chen, C. Z. Dong, J. Jiang and L. Y. Xie, *J. Phys. B* **48** 144030 (2015).
- [30] B. K. Sahoo, *J. Phys. B* **43**, 231001 (FTC) (2010).
- [31] D. K. Nandy, S. Singh and B. K. Sahoo, *MNRAS* **452**, 2546 (2015).
- [32] B. K. Sahoo and B. P. Das, *Phys. Rev. A* **92**, 052511 (2015).
- [33] B. K. Sahoo, *Phys. Rev. A* **93**, 022503 (2016).
- [34] E. Charro and I. Martín, *Astrophys. J.* **585**, 1191 (2003).
- [35] A. G. Jensen and T. P. Snow, *Astrophys. J.* **669**, 401 (2007).
- [36] G. Çelik, D. Doğan, Ş. Ateş, and M. Taşer, *J. Quant. Spectrosc. Radiat. Transfer* **113**, 1601 (2012).
- [37] N. F. Allard, G. Guillon, V. A. Alekseev and J. F. Kielkopf, *A & A* **593**, A13 (2016).
- [38] M. Guitou, A. K. Belyaev, P. S. Barklem, A. Spielfiedel and N. Feautrier, *J. Phys. B* **44**, 035202 (2011).
- [39] L. Sharma, A. Surzhykov, R. Srivastava, S. Fritzsche, *Phys. Rev. A* **83**, 062701 (2011).
- [40] S. J. Smith, A. Chutjian, J. Mitroy, S. S. Tayal, R. J. W. Henry, K-F. Man, R. J. Mawhorter, and I. D. Williams, *Phys. Rev. A* **48**, 292 (1993).
- [41] I. D. William, A. Chutjian, and R. J. Mawhorter, *J. Phys. B* **19**, 2189 (1986).
- [42] I. D. Williams, A. Chutjian, A. Z. Msezane, and R. J. W. Henry, *Astrophys. J.* **299**, 1063 (1985).
- [43] Y. K. Kim, *Phys. Rev. A* **65**, 022705 (2002).
- [44] A. W. Pangantiwar and R. Srivastava, *J. Phys. B* **21**, L219 (1988).
- [45] M. Das, B. K. Sahoo, and S. Pal, *Phys. Rev. A* **93**, 052513 (2016).
- [46] B. K. Sahoo and M. Das, *Eur. Phys. J. D* **70**, 270 (2016).
- [47] [<http://www.nist.gov/pml/data/asd.cfm>].
- [48] F. A. Parpia, C. F. Fischer, and I. P. Grant, *Comput. Phys. Commun.* **94**, 249 (1996).
- [49] [<http://aphysics2.lanl.gov/cgi-bin/ION/runlanl08d.pl>].